Chemical Science

EDGE ARTICLE

Mode selectivity in methane dissociative chemisorption on Ni(111)†

Bin Jiang,‡[a] Rui Liu,‡[b] Jun Li,[a] Daiqian Xie,*[c] Minghui Yang*[b] and Hua Guo*[a]

Dissociative chemisorption of CH_4 on transition-metal surfaces, representing the rate-limiting step in methane steam reforming, has been shown experimentally to be strongly mode selective. To understand the mode selectivity, a twelve-dimensional global potential energy surface is developed for CH_4 interacting with a rigid Ni(111) surface based on a large number of density functional theory points. The reaction dynamics is investigated using an eight-dimensional quantum model, which includes representatives of all four vibrational modes of methane. After correcting for surface effects, key experimental observations, including the mode selectivity, are well reproduced. These theoretical results, along with mechanistic analysis, provide insights into this industrially important heterogeneous reaction.

A central question in chemistry is how to control reactivity and product branching. Thanks to the quantum mechanical nature of molecular systems, it is possible to manipulate the reactivity by selectively exciting certain internal modes of the reactant using lasers.[1,2] Such mode selective chemistry has been experimentally demonstrated for several reactions in the gas phase[2] and on surfaces.[3] Despite recent advances,[4–7] our theoretical understanding of the key factors that influence the mode selectivity still lags significantly behind.[8] This was clearly reflected in the case of the $F + CHD_3$ reaction at low collision energies,[9,10] where pre-reaction van der Waals forces were found to steer the system towards a saddle point not favored by Polanyi's rules.[11] The slow progress can be largely attributed to the lack of global potential energy surfaces (PESs) and difficulties in modeling high-dimensional quantum dynamics.[12,13]

The activated dissociative chemisorption of CH_4 on Ni(111) forming adsorbed CH_3 and H is not only of industrial importance as the rate-limiting step in methane steam reforming,[14] but also a prototype for understanding heterogeneous catalysis on transition-metal surfaces.[3,13] The four vibrational modes in CH_4 endow it with richer chemistry than the well-studied dissociative chemisorption of H_2.[15,16] Experimentally, its

quantum state-resolved reactivity has been shown to vary widely.[3] While rotational excitation seems to have a limited effect,[17] the excitation of methane stretching modes greatly enhances the reactivity, sometimes more efficiently than translational energy.[18–25] In particular, the symmetric stretch (ν_1) is more efficient than asymmetric stretch (ν_3), while the umbrella (ν_4) mode enhances the reaction with less potency.[23]

An in-depth understanding of these experimentally observed strong mode selectivities requires theoretical interpretation. The non-statistical nature of the reaction underscores the importance of dynamics. Recent *ab initio* direct dynamics work has shed some light on the intramolecular energy flow and mode selectivity in methane dissociative chemisorption.[26,27] While no potential energy surface (PES) was needed, the classical representation of the dynamics in these studies cannot describe tunneling, which plays a dominant role at low energies. While insightful, the trajectories were sampled from the transition state, thus yielding attributes that cannot be directly compared with experiment. To quantitatively describe the reactive scattering process, an accurate global PES is needed. So far, however, this effort has been fraught with difficulties due to the large number of degrees of freedom involved.[13] Indeed, even with the rigid surface approximation, fifteen coordinates are needed to describe the CH_4/Ni system. With the exception of an early semi-empirical PES,[28] it is only recently that semi-global[29–31] and global[32] full-dimensional PESs have started to emerge. Even with such a PES, an accurate quantum description of the reaction dynamics remains a formidable task.[13] Indeed, most previous dynamical studies have relied on low-dimensional models,[32–42] many treating CH_4 as a quasi-diatom or quasi-triatom. These models are incapable of addressing important issues such as the relative efficacy of the symmetric *vs.* asymmetric stretching modes in promoting the reaction. The only full-dimensional dynamical studies of Jackson and Nave,[30,31] while shedding

aDepartment of Chemistry and Chemical Biology, University of New Mexico, Albuquerque, New Mexico, 87131, USA. E-mail: hguo@unm.edu

bKey Laboratory of Magnetic Resonance in Biological Systems, State Key Laboratory of Magnetic Resonance and Atomic and Molecular Physics, Wuhan Centre for Magnetic Resonance, Wuhan Institute of Physics and Mathematics, Chinese Academy of Sciences, Wuhan 430071, China. E-mail: yangmh@wipm.ac.cn

cInstitute of Theoretical and Computational Chemistry, Key Laboratory of Mesoscopic Chemistry, School of Chemistry and Chemical Engineering, Nanjing University, Nanjing 210093, China. E-mail: dqxie@nju.edu.cn

† Electronic supplementary information (ESI) available. See DOI: 10.1039/c3sc51040a

‡ Equal contributions.

valuable light on the dynamics, were based on the approximate reaction path Hamiltonian[43] and systematically underestimated the vibrational efficacy for each mode.

In this publication, we present a twelve-dimensional (12D) global PES for CH_4 on Ni(111) based on a large number of density functional theory (DFT) calculations. As in previous theoretical investigations,[32–42] our model assumes that the dissociative chemisorption of CH_4 is electronically adiabatic and the surface electron–hole pair excitations are unimportant. We chose to ignore the CH_4 center of mass (COM) translational motion along the surface plane (X and Y) as well as the azimuthal angle (ϕ) about the surface normal (Z), because these coordinates are not critical to the reaction.[33] The neglect of the lateral coordinates is consistent with the observed "normal energy scaling" in methane dissociative chemisorption on transition metal surfaces,[3] namely the fact that the sticking probability depends only on the kinetic energy along the surface normal. On the other hand, the surface corrugation is expected to affect the reactivity, and it is approximately taken into consideration as discussed below and in more detail in the ESI.†

In the DFT calculations, the Ni(111) surface was approximated using a three-layer slab with an inter-slab separation of 12 Å. The CH_4 molecule was placed above a 2×2 (1/4 ML coverage) surface unit cell. The interaction between the ionic cores and electrons was described with the projector-augmented wave (PAW) method,[44] and the Kohn–Sham valence electronic wavefunction was expanded in a plane-wave basis set[45] with a cutoff at 350 eV. The electron exchange-correlation effects were treated within the generalized gradient approximation (GGA),[46] using the Perdew–Wang (PW91) functional.[47] The Brillouin zone was sampled with a $3 \times 3 \times 1$ Monkhorst–Pack k-points grid mesh.[48] As in most previous theoretical studies of the CH_4/Ni system,[29,30,32,39,40,49] the spin-polarized model was used in order to provide an accurate account of the reaction barrier. The optimized lattice constant for bulk Ni obtained in this work (3.518 Å) is in excellent agreement with the experimental value (3.524 Å).[50] In the calculations reported below, all surface atoms were fixed at their equilibrium positions. As shown in the ESI,† extensive convergence tests were performed and this model was found to be accurate in describing the stationary points along the reaction path for methane dissociative chemisorption. All plane-wave DFT calculations were performed with the Vienna Ab initio Simulation Package (VASP).[51,52]

Following our previous work on H_2O/Cu(111),[53–55] we employed the permutation invariant polynomial approach of Bowman and coworkers[56] to construct the PES. To this end, we introduced a *pseudo* "surface atom" in addition to the C atom and four H atoms, and represented the PES by a polynomial expansion in Morse-like variables ($y_{ij} = \exp(-r_{ij}/a)$ with $a = 2.0$ Bohr) of interatomic distances (r_{ij}) among the six atoms:

$$V = \sum_{\{l_{ij}\}} c_{\{l_{ij}\}} \hat{S} \prod_{i<j}^{6} y_{ij}^{l_{ij}} \quad (1)$$

where $\hat{S}$ is the symmetrization operator to make the polynomial basis invariant under permutations of like atoms, and l_{ij} is the order of each Morse monomial. The "surface atom" was placed

at the vertical projection of the CH_4 COM. We included all terms with the total order not exceeding 6, leading to 3250 terms. The expansion coefficients were then determined by a weighted least squares method, in which a configuration with energy E has a weight as $w = E/(E + E_0)$ for $E_0 = 144.7$ kJ mol^{-1}. It is worth noting that the absence of the lateral coordinates (X, Y) in our model renders the PES less reliable in the product channel,[53] but its faithful characterization of the reactant valley and transition state in the PES was sufficient for our purposes here.

A total of 36 597 DFT points were generated and most of these points were distributed in the normal mode coordinates along the reaction path. In order to give a better description of the stationary points, the weights for points near the CH_4 asymptote and the transition state were increased by a factor of 5 and 8, respectively. The overall RMSD (root mean square deviation) for the fit is 5.6 kJ mol^{-1}, but the RMSD is significantly smaller (1.92 kJ mol^{-1}) for points below 145 kJ mol^{-1} relative to global minimum.

The PES is displayed in Fig. 1 as a function of the molecule–surface distance (Z) and the H–CH_3 distance (r), with all other coordinates relaxed. It is clear that this reaction has a "late" barrier, which is about 105 kJ mol^{-1} above the reactant asymptote, in agreement with previous theoretical calculations.[29,39,40,57,58]

Due to the tunneling nature of the reaction and large zero-point energies, a quantum method is needed for an accurate description of the reaction dynamics. Unfortunately, it is still extremely difficult to characterize quantum reactive scattering in twelve dimensions. We have thus resorted to an eight-dimensional (8D) model for CH_4 interacting with a rigid Ni(111) surface based on a slightly modified[59] Palma–Clary Hamiltonian for $X + YCZ_3 \rightarrow XY + CZ_3$ type reactions,[60] which has been successfully applied to many $X + CH_4$ reactions.[5,59,61–64] The restriction of the non-reactive CZ_3 moiety to C_{3v} represents a sensible approximation as the methyl moiety maintains its C_{3v} symmetry reasonably well along the reaction coordinate. This 8D model is a significant advance over previous reduced-dimensional models as it includes representatives of all CH_4 vibrational modes.
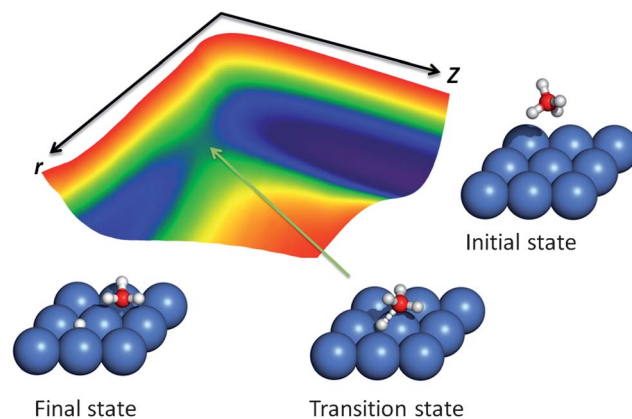

Fig. 1 Potential energy surface for CH_4 on Ni(111) as a function of the distance between the CH_4 center of mass and the surface (Z) and the distance between the dissociating H atom and CH_3 center of mass (r). All other coordinates are relaxed. The configurations of the stationary points are illustrated in the figure.

The 8D model Hamiltonian for the dissociative chemisorption of CH_4 on Ni(111) is given by ($\hbar = 1$)

$$\hat{H} = -\frac{1}{2M_{CH_4}}\frac{\partial^2}{\partial Z^2} - \frac{1}{2\mu_r}\frac{\partial^2}{\partial r^2} + \frac{\hat{l}^2}{2\mu_r r^2} + \hat{K}^{vib}_{CH_3} + \hat{K}^{rot}_{CH_3}$$
$$+ V(Z, r, x, s, \theta_1, \varphi_1, \theta_2, \varphi_2), \quad (2)$$

where Z is the distance between the CH_4 COM and the surface and r the distance between the atom H and CH_3 COM, with M_{CH_4} and μ_r as the mass of CH_4 and H–CH_3 reduced mass. As shown in Fig. 2, (θ_1, φ_1) are angles that define the rotation of CH_4 with respect to Z and (θ_2, φ_2) are angles that define the rotation of CH_3 with respect to r. $\hat{l} = \hat{J} - \hat{j}$ is the orbital angular momentum of atom H with respect to CH_3, with $\hat{J}$ and $\hat{j}$ as the rotational angular momenta of CH_4 and CH_3.

The CH_3 vibration can be described in either the Cartesian coordinates (x, s) or scaled polar coordinates (q, γ).[59] The coordinate q describes the CH bond stretch and γ for the umbrella vibration of CH_3 moiety, respectively. They are related to x and s via the following expressions:

$$q = \sqrt{x^2 + \frac{m_C}{m_C + 3m_H}s^2}, \quad \gamma = \arctan\left(\sqrt{\frac{m_C}{m_C + 3m_H}}\frac{s}{x}\right), \quad (3)$$

with the integral element as $dq\,d\gamma$. In the (q, γ) coordinate system, the vibrational and rotational kinetic energy operators of CH_3, $\hat{K}^{vib}_{CH_3}$ and $\hat{K}^{rot}_{CH_3}$, have the following form:

$$\hat{K}^{vib}_{CH_3} = -\frac{1}{6m_H}\left(\frac{\partial^2}{\partial q^2} + \frac{1}{q^2}\frac{\partial^2}{\partial \gamma^2} + \frac{1}{4q^2}\right), \quad (4)$$

$$\hat{K}^{rot}_{CH_3} = \frac{1}{2I_A}\hat{j}^2 + \left(\frac{1}{2I_C} - \frac{1}{2I_A}\right)\hat{j}_s^2, \quad (5)$$

where $\hat{j}_s$ is the projection of $\hat{j}$ on to $\hat{S}$ which is the C_{3v} symmetry axis of CH_3 moiety as defined in Fig. 2. I_A and I_C are the rotational inertias of the CH_3 moiety:

$$I_A = \frac{3}{2}m_H\left[x^2 + \frac{2m_C}{m_C + 3m_H}s^2\right], \quad I_C = 3m_H x^2. \quad (6)$$

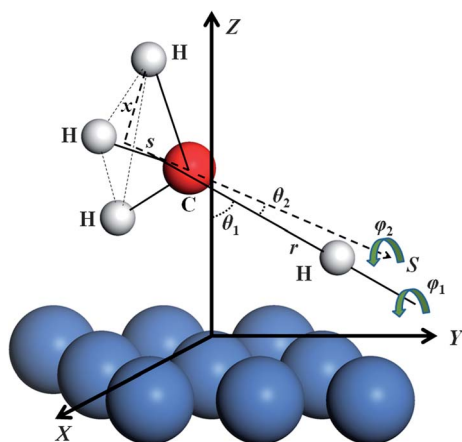The wave packet is expanded in terms of the basis sets for Z, r, q, γ and the rotational basis functions.

Fig. 2 Coordinates used in the 8D quantum dynamical model.

$$\Psi = \sum_{n_Z, n_r, n_q, n_\gamma} \sum_{Jljk} c_{n_Z n_r n_q n_\gamma Jljk}(t) G_{n_Z}(Z) F_{n_r}(r) Q_{n_q}(q) H_{n_\gamma}(\gamma) \Phi_{Jljk}(\hat{r}, \hat{S}), \quad (7)$$

where k is the projection of j onto the C_{3v} symmetry axis $\hat{S}$. The rotational basis function is expressed as

$$\Phi_{Jjlk}(\hat{r}, \hat{S}) = \sum_m \overline{D}^J_{Mm}(\hat{r})\sqrt{\frac{2l+1}{2J+1}}\langle jml\,0|Jm\rangle \overline{D}^j_{mk}(\hat{S}), \quad (8)$$

where m is the projection of J onto the H–CH_3 axis, $\overline{D}^J_{mk}$ is the normalized Wigner rotational matrix and $\langle jmj'm'|JM\rangle$ the Clebsch–Gordan coefficient.[65] M is the projection of J on the surface normal, and is conserved since the PES does not depend on the azimuthal angle. Here, it is chosen to be zero since only the $J = 0$ case is considered.

The time-dependent Schrödinger equation was solved using the split-operator method,[66] with an initial Gaussian wave packet associated with a particular ro-vibrational state of CH_4:

$$\Psi(t = 0) = N e^{-(Z - Z_0)^2/\alpha} e^{ik_0 Z}\psi_{CH_4}, \quad (9)$$

where N, Z_0, α, k_0 are respectively the normalization factor, position, half-width, and central energy of the Gaussian wave packet. ψ_{CH_4} is the ro-vibrational wave function of CH_4, which has been pre-determined in the reactant asymptote and solved with a five-dimensional model. The vibrational quantum numbers are labeled by (n_1, n_2, n_3, n_4) for the symmetric stretching, bending, asymmetric stretching and umbrella modes of CH_4, respectively.

The total reaction probability is obtained at a dividing surface placed as $r = 3.5$ Bohr using a flux formalism.[67] An L-shaped expansion[68] for Z and r was used to reduce the size of the basis set. A total of 300 sine basis functions ranging from 3.0 to 10.0 Bohr were used for the Z basis set expansion with 130 nodes in the interaction region; and 6 and 30 basis functions of r were used in the asymptotic and interaction regions, respectively. For the vibration of CH_3 group, the q and γ coordinates are each described by 5 basis functions. The size of the rotational basis functions is controlled by the parameters, $J_{max} = 51$, $l_{max} = 30$, $j_{max} = 21$ and $k_{max} = 3$. Both OpenMP and MPI parallelization were used to render the computational costs manageable. It is worth noting that the probabilities obtained in the wave packet calculations are multiplied by a factor of 4 to account for the four equivalent C–H bonds.

Our rigid-surface model ignores the motion of surface atoms and energy transfer between the impinging molecule and surface phonons, both representing severe approximations. Indeed, it is well known that the CH_4 dissociative chemisorption on Ni depends on the surface temperature,[69–71] suggesting the involvement of surface atoms. Jackson and coworkers have investigated these effects extensively and carefully,[30,38–42] and we follow primarily their approaches, as detailed in the ESI.† In particular, three corrections have been made. First, the surface corrugation is approximately taken into account by averaging higher-energy sites using an energy shifting model.[30] This correction lowers the reaction probabilities due to a higher effective barrier. Second, the so-called "electronic coupling",

which manifests in terms of the "puckering" of a surface Ni atom at the transition state, is modeled with a Boltzmann sampling of its position[42] at the experimental temperature of 475 K.[3] This correction has a large impact on the reaction probabilities at low collision energies, due to the lower reaction barrier with the "puckered" surface Ni atom.[38–40] Finally, the "mechanical coupling", which originates from the vibration of the surface Ni atom, is approximated by a surface mass model.[33,42]

The calculated reaction probabilities are compared in Fig. 3 with the measured initial sticking probabilities (S_0) for various CH$_4$ vibrational states. The theory–experiment agreement is quite good, which provides supporting evidence for the validity of the PES and reduced-dimensional model. It also lends support to the notion that this reaction is electronically adiabatic.

While the exponentially increasing reactivity with the collision energy along the surface normal (E_Z) shown in Fig. 3 clearly illustrates the effect of translational energy, the role of vibrational excitation is less obvious. To quantify the promotional effects, it is customary to define the vibrational efficacy as follows:

$$\eta = \frac{E_Z(0, S_0) - E_Z(v, S_0)}{\Delta E_v}, \qquad (10)$$

where ΔE_v the energy difference between ground (0) and excited (v) vibrational levels in CH$_4$. Thus, an η value larger than 1.0 would indicate that the vibrational energy is more efficient than translational energy in promoting the reaction, and *vice versa*. In Table 1, the calculated vibrational efficacies of various excited CH$_4$ states compare well with the available experimental data.[3] In particular, the symmetric stretch (v_1) is the most effective in promoting reaction, followed by the asymmetric stretch (v_3). Both are more effective than translational energy. These observations are consistent with Polanyi's rules,[11] which predict high vibrational efficacy for stretching vibrations in
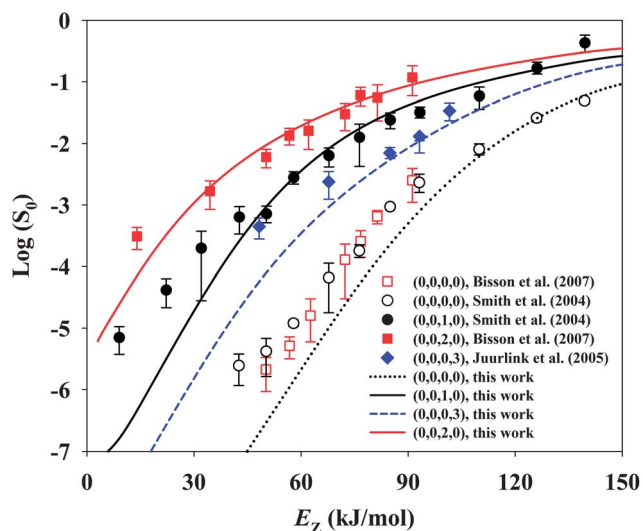
reactions with a "late" barrier. Interestingly, the excitation to the second overtone of the asymmetric stretching ($2v_3$) mode becomes less effective than the translational energy. On the other hand, the umbrella (n_4v_4 with $n_4 = 1, 2, 3$) mode of CH$_4$ is much less potent in promoting the reaction. The different vibrational efficacies underscore the complexity of the multi-dimensional reaction dynamics and the way in which the vibrational modes are coupled with the reaction coordinate.

The dramatic mode selectivity observed in experiment and reproduced here theoretically can be understood, at least partially, with a vibrationally adiabatic model[29,30,36] based on the reaction path Hamiltonian.[43] To this end, the minimum energy path (MEP) and generalized normal modes along the reaction coordinate are determined on the DFT based PES, as detailed in the ESI.† As CH$_4$ approaches the surface, the symmetric stretching and umbrella modes "soften", reflected by a large drop in their frequencies, due to their strong coupling with the reaction coordinate.[36] As a result, the corresponding barriers for these "reactive" modes are lowered from that for the ground vibrational state, leading to enhanced reactivity. On the other hand, the three-fold degenerate asymmetric stretch is a "spectator" mode, as its frequencies are largely unchanged during the reaction. Consequently, the corresponding adiabatic barriers are roughly the same as those of the vibrational ground state. Its observed enhancement is likely to stem from vibrational non-adiabaticity, which channels energy into the reaction coordinate[30] or other modes.[29,36] This is evidenced by the small but non-zero couplings with the reaction coordinate on our PES, as discussed in the ESI.† Non-adiabatic transitions between the symmetric and asymmetric stretching modes are also present in the entrance channel, as illustrated by a significant Massey parameter[72] in the recent analyses.[29,36] On our PES, the Massey parameters range from 0.36 to 0.57 depending on the initial collision energy, clearly implying strong vibrational non-adiabaticity in this system.

While the above adiabatic picture provides some insights, a sudden model offers a complementary explanation of the mode selectivity due to the large kinetic energy of the impinging molecule. We have developed a Sudden Vector Projection (SVP) model,[73] as detailed in the ESI,† in which overlaps of the CH$_4$ normal mode vectors with the reaction coordinate vector at the transition state are calculated. The excitation in a specific CH$_4$

Fig. 3 Comparison of calculated and measured initial sticking coefficients (S_0) for various vibrational states of CH$_4$ as a function of the collision energy.

Table 1 Comparison between calculated and measured vibrational efficacies for several low-lying excited vibrational states of CH$_4$ in its dissociative chemisorption on Ni(111)

(n_1,n_2,n_3,n_4)	E_v (cm^{-1})	SVP	$S_0 = 10^{-5}$	$S_0 = 10^{-4}$	$S_0 = 10^{-3}$	Expt.[a]
			Vibrational efficacy η			
(0,0,0,1)	1259	0.204	0.40	0.41	0.41	—
(0,0,0,2)	2506	—	0.67	0.63	0.55	—
(1,0,0,0)	2889	0.396	1.23	1.28	1.34	1.40[b]
(0,0,1,0)	2939	0.314	1.15	1.20	1.26	1.25
(0,0,0,3)	3748	—	0.64	0.63	0.59	0.72
(0,0,2,0)	5808	—	0.90	0.93	0.94	0.90

[a] Experimental data taken from ref. 3. [b] This data point measured on Ni(100) is included for qualitative comparison because of the lack of data on Ni(111).

vibrational mode enhances the reaction by having a good overlap with the reaction coordinate in the sudden limit. Our model predicts the vibrational efficacy in the order: $\nu_1 > \nu_3 > \nu_2 > \nu_4$, as shown by the overlaps listed in Table 1, in agreement with both theoretical and experimental observations. An important prediction from the SVP model is that the two stretching modes provide roughly the same enhancement, without invoking vibrational non-adiabaticity. A similar conclusion was also reached by Sacchi et al.[26]

In summary, our high-dimensional quantum dynamical model on a DFT based PES is shown to reproduce most experimental observations in the dissociative chemisorption of CH_4 on Ni(111). Despite its reduced-dimensional nature, the 8D model includes representatives of all vibrational modes of CH_4, thus allowing the treatment of all mode selectivities on an equal footing. The theory–experiment agreement underscores the accuracy of the PES and the capacity of the 8D dynamical model for capturing key features of this important and challenging heterogeneous catalytic reaction. Furthermore, analyses suggest that the selectivity is largely dictated by the coupling of reactant vibrational modes with the reaction coordinate at the "late" transition state. We note in passing that the model used here can be readily extended to understand bond selectivity[74] and stereo-dynamics[75] of this reaction.

Acknowledgements

References

1 R. N. Zare, *Science*, 1998, **279**, 1875.

2 F. F. Crim, *Acc. Chem. Res.*, 1999, **32**, 877.

3 L. B. F. Juurlink, D. R. Killelea and A. L. Utz, *Prog. Surf. Sci.*, 2009, **84**, 69.

4 G. Czakó and J. M. Bowman, *Science*, 2011, **334**, 343.

5 Z. Zhang, Y. Zhou, D. H. Zhang, G. Czakó and J. M. Bowman, *J. Phys. Chem. Lett.*, 2012, **3**, 3416.

6 J. Li, B. Jiang and H. Guo, *J. Am. Chem. Soc.*, 2013, **135**, 982.

7 B. Fu and D. H. Zhang, *J. Chem. Phys.*, 2013, **138**, 184308.

8 S. Yan, Y.-T. Wu and K. Liu, *Proc. Natl. Acad. Sci. U. S. A.*, 2008, **105**, 12667.

9 W. Zhang, H. Kawamata and K. Liu, *Science*, 2009, **325**, 303.

10 G. Czakó and J. M. Bowman, *J. Am. Chem. Soc.*, 2009, **131**, 17534.

11 J. C. Polanyi, *Science*, 1987, **236**, 680.

12 S. C. Althorpe and D. C. Clary, *Annu. Rev. Phys. Chem.*, 2003, **54**, 493.

13 G.-J. Kroes, *Phys. Chem. Chem. Phys.*, 2012, **14**, 14966.

14 J. R. Rostrup-Nielsen, in *Catalysis, Science and Technology*, ed. J. R. Anderson and M. Boudart, Springer-Verlag, Berlin, 1984, vol. 5.

15 A. Gross, *Surf. Sci. Rep.*, 1998, **32**, 291.

16 G.-J. Kroes, *Prog. Surf. Sci.*, 1999, **60**, 1.

17 L. B. F. Juurlink, R. R. Smith and A. L. Utz, *Faraday Discuss.*, 2000, **117**, 147.

18 L. B. F. Juurlink, P. R. MaCabe, R. R. Smith, C. L. DeCologero and A. L. Utz, *Phys. Rev. Lett.*, 1999, **83**, 868.

19 J. Higgins, A. Conjusteau, G. Scoles and S. L. Bernasek, *J. Chem. Phys.*, 2001, **114**, 5277.

20 M. P. Schmid, P. Maroni, R. D. Beck and T. R. Rizzo, *J. Chem. Phys.*, 2002, **117**, 8603.

21 R. D. Beck, P. Maroni, D. C. Papageorgopoulos, T. T. Dang, M. P. Schmid and T. R. Rizzo, *Science*, 2003, **302**, 98.

22 R. R. Smith, D. R. Killelea, D. F. DelSesto and A. L. Utz, *Science*, 2004, **304**, 992.

23 L. B. F. Juurlink, R. R. Smith, D. R. Killelea and A. L. Utz, *Phys. Rev. Lett.*, 2005, **94**, 208303.

24 P. Maroni, D. C. Papageorgopoulos, M. Sacchi, T. T. Dang, R. D. Beck and T. R. Rizzo, *Phys. Rev. Lett.*, 2005, **94**, 246104.

25 R. Bisson, M. Sacchi, T. T. Dang, B. Yoder, P. Maroni and R. D. Beck, *J. Phys. Chem. A*, 2007, **111**, 12679.

26 M. Sacchi, D. J. Wales and S. J. Jenkins, *J. Phys. Chem. C*, 2011, **115**, 21832.

27 M. Sacchi, D. J. Wales and S. J. Jenkins, *Phys. Chem. Chem. Phys.*, 2012, **14**, 15879.

28 S. E. Wonchoba and D. G. Truhlar, *J. Phys. Chem. B*, 1998, **102**, 6842.

29 G. P. Krishnamohan, R. A. Olsen, A. Valdes and G.-J. Kroes, *Phys. Chem. Chem. Phys.*, 2010, **12**, 7654.

30 B. Jackson and S. Nave, *J. Chem. Phys.*, 2011, **135**, 114701.

31 B. Jackson and S. Nave, *J. Chem. Phys.*, 2013, **138**, 174705.

32 G. P. Krishnamohan, R. A. Olsen, G.-J. Kroes, F. Gatti and S. Woittequand, *J. Chem. Phys.*, 2010, **133**, 144308.

33 A. C. Luntz and J. Harris, *Surf. Sci.*, 1991, **258**, 397.

34 A. P. J. Jansen and H. Burghgraef, *Surf. Sci.*, 1995, **344**, 149.

35 M.-N. Carre and B. Jackson, *J. Chem. Phys.*, 1998, **108**, 3722.

36 L. Halonen, S. L. Bernasek and D. J. Nesbitt, *J. Chem. Phys.*, 2001, **115**, 5611.

37 Y. Xiang, J. Z. H. Zhang and D. Y. Wang, *J. Chem. Phys.*, 2002, **117**, 7698.

38 S. Nave and B. Jackson, *Phys. Rev. Lett.*, 2007, **98**, 173003.

39 S. Nave and B. Jackson, *J. Chem. Phys.*, 2007, **127**, 224702.

40 S. Nave and B. Jackson, *J. Chem. Phys.*, 2009, **130**, 054701.

41 A. K. Tiwari, S. Nave and B. Jackson, *Phys. Rev. Lett.*, 2009, **103**, 253201.

42 A. K. Tiwari, S. Nave and B. Jackson, *J. Chem. Phys.*, 2010, **132**, 134702.

43 W. H. Miller, N. C. Handy and J. E. Adams, *J. Chem. Phys.*, 1980, **72**, 99.

44 P. E. Blöchl, *Phys. Rev. B: Condens. Matter*, 1994, **50**, 17953.

45 G. Kresse and D. Joubert, *Phys. Rev. B: Condens. Matter Mater. Phys.*, 1999, **59**, 1758.

46 J. P. Perdew, K. Burke and M. Ernzerhof, *Phys. Rev. Lett.*, 1996, **77**, 3865.

47 J. P. Perdew, J. A. Chevary, S. H. Vosko, K. A. Jackson, M. R. Pederson, D. J. Singh and C. Fiolhais, *Phys. Rev. B: Condens. Matter*, 1992, **46**, 6671.

48 H. J. Monkhorst and J. D. Pack, *Phys. Rev. B: Solid State*, 1976, **13**, 5188.

49 S. Nave, A. K. Tiwari and B. Jackson, *J. Chem. Phys.*, 2010, **132**, 054705.

50 D. R. Lide, *CRC Handbook of Chemistry and Physics*, Internet Version 2005, CRC Press, Boca Raton, FL, 2005.

51 G. Kresse and J. Furthmuller, *Phys. Rev. B: Condens. Matter*, 1996, **54**, 11169.

52 G. Kresse and J. Furthmuller, *Comput. Mater. Sci.*, 1996, **6**, 15.

53 B. Jiang, X. Ren, D. Xie and H. Guo, *Proc. Natl. Acad. Sci. U. S. A.*, 2012, **109**, 10224.

54 B. Jiang, D. Xie and H. Guo, *Chem. Sci.*, 2013, **4**, 503.

55 B. Jiang, J. Li, D. Xie and H. Guo, *J. Chem. Phys.*, 2013, **138**, 044704.

56 J. M. Bowman, G. Czakó and B. Fu, *Phys. Chem. Chem. Phys.*, 2011, **13**, 8094.

57 P. Kratzer, B. Hammer and J. K. Nørskov, *J. Chem. Phys.*, 1996, **105**, 5595.

58 G. Henkelman, A. Arnaldsson and H. Jónsson, *J. Chem. Phys.*, 2006, **124**, 044706.

59 R. Liu, H. Xiong and M. Yang, *J. Chem. Phys.*, 2012, **137**, 174113.

60 J. Palma and D. C. Clary, *J. Chem. Phys.*, 2000, **112**, 1859.

61 M. Yang, D. H. Zhang and S.-Y. Lee, *J. Chem. Phys.*, 2002, **117**, 9539.

62 M. Yang, S.-Y. Lee and D. H. Zhang, *J. Chem. Phys.*, 2007, **126**, 064303.

63 W. Zhang, Y. Zhou, G. Wu, Y. Lu, H. Pan, B. Fu, Q. Shuai, L. Liu, S. Liu, L. Zhang, B. Jiang, D. Dai, S.-Y. Lee, Z. Xie, B. J. Braams, J. M. Bowman, M. A. Collins, D. H. Zhang and X. Yang, *Proc. Natl. Acad. Sci. U. S. A.*, 2010, **107**, 12782.

64 R. Liu, M. Yang, G. Czakó, C. T. Bowman, J. Li and H. Guo, *J. Phys. Chem. Lett.*, 2012, **3**, 3776.

65 R. N. Zare, *Angular Momentum*, Wiley, New York, 1988.

66 M. D. Feit, J. A. Fleck and A. Steger, *J. Comput. Phys.*, 1982, **47**, 412.

67 D. H. Zhang and J. Z. H. Zhang, *J. Chem. Phys.*, 1994, **100**, 2697.

68 R. C. Mowrey, *J. Chem. Phys.*, 1991, **94**, 7098.

69 M. B. Lee, Q. Y. Yang and S. T. Ceyer, *J. Chem. Phys.*, 1987, **87**, 2724.

70 P. M. Holmblad, J. Wambach and I. Chorkendorff, *J. Chem. Phys.*, 1995, **102**, 8255.

71 D. R. Killelea, V. L. Campbell, N. S. Shuman and A. L. Utz, *J. Phys. Chem. C*, 2009, **113**, 20618.

72 M. S. Child, *Molecular Collision Theory*, Academic Press, London, 1974.

73 B. Jiang and H. Guo, *J. Chem. Phys.*, 2013, in press.

74 D. R. Killelea, V. L. Campbell, N. S. Shuman and A. L. Utz, *Science*, 2008, **319**, 790.

75 B. L. Yoder, R. Bisson and R. D. Beck, *Science*, 2010, **329**, 553.